SUPPLEMENTARY INFORMATION

Understanding Ligand-Exchange Reactions on Thiolate-Protected Gold Clusters by Probing Isomer Distributions Using Reversed-Phase High-Performance Liquid Chromatography

Yoshiki Niihori,[†] Yoshihiro Kikuchi,[†] Ayano Kato,[†] Miku Matsuzaki,[†] and Yuichi Negishi[†,‡,#,*]

[†]Department of Applied Chemistry, Faculty of Science, Tokyo University of Science, 1-3 Kagurazaka, Shinjuku-ku, Tokyo 162−8601, Japan

[‡]Photocatalysis International Research Center, Tokyo University of Science, 2641 Yamazaki, Noda, Chiba 278−8510, Japan

[#]Department of Materials Molecular Science, Institute for Molecular Science, Myodaiji, Okazaki, Aichi 444−8585, Japan

I. Counting method for the number of repetitions of site combinations for each isomer of $Au_{24}Pd(SC_2H_4Ph)_{18-n}(SC_{12}H_{25})_n$ (n = 1,2).

The number of repetitions of site combinations for each isomer of $Au_{24}Pd(SC_2H_4Ph)_{18-n}(SC_{12}H_{25})_n$ (n = 1,2) shown in Figure 7(a)(b) (vertical axis of Figure 7(c)(d)) was calculated using the orbit-stabilizer theorem[1]. In this calculation, $Au_{24}Pd(SR)_{18}$ was assumed to be symmetrical for T_h ={E, $4C_3$, $4C_3^2$, $3C_2$', i, $4S_6$, $4S_6^5$, $3\sigma_h$} (Chart S1), which has the order of 24. The point groups and orders of the isomers of the isomer index i = 1,2 and j = 1–12 are summarized in Table S2. The number of repetitions of site combinations can be calculated by dividing 24 by the number of the order. For example, the order of the isomer of index j = 3 is 4, since it has a symmetry of C_{2v} (Table S2). Thus, the number of repetitions of site combinations for this isomer is 6 (Chart S2), which is calculated by dividing 24 by 4. These calculations give values of the number of repetitions of site combinations shown in Table S2 for isomers of the isomer index i = 1,2 and j = 1–12.

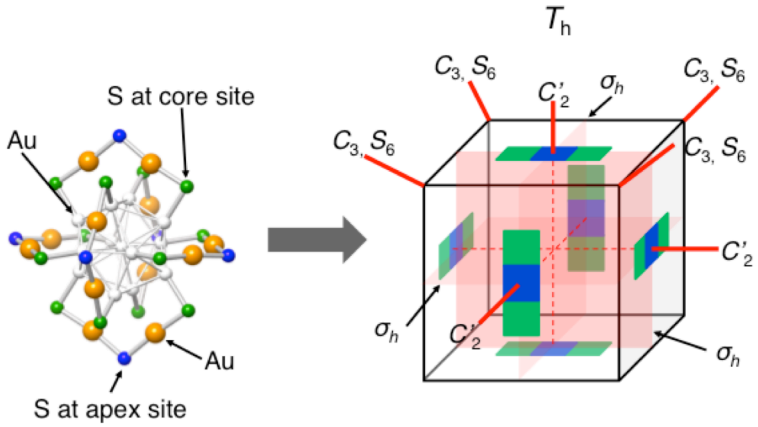

Chart S1. Simplification of $Au_{24}Pd(SR)_{18}$ structure used to calculate the number of repetitions of site combinations. The green and blue squares indicate the core and apex sulfurs, respectively.

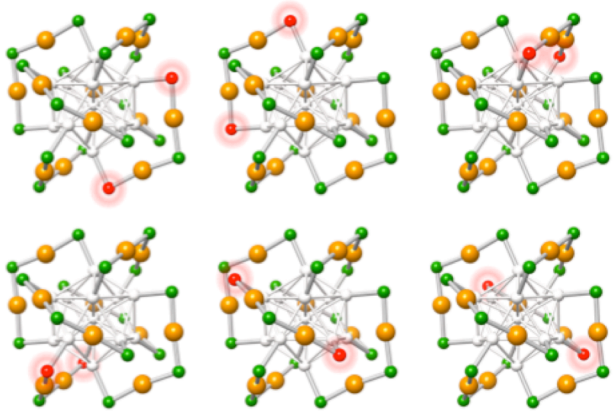

Chart S2. Six site combinations for isomer of $Au_{24}Pd(SC_2H_4Ph)_{16}(SC_{12}H_{25})_2$ of j = 3.

II. Data

Table S1. Various solvent properties.

solvent	role in the experiment [a]	ε_r [b]	η (mPa s) [c]
acetonitrile	adsorption solvent	36.8 [d]	0.369
methanol	adsorption solvent	33.5 [d]	0.544
acetone	elution solvent	21.1 [d]	0.306
tetrahydrofuran	elution solvent	7.57 [d]	0.456

[a]See the text. [b]Dielectric constant at 20 °C.[2] [c]Viscosity at 25 °C.[2] [d]ε_r of these solvents are lower than ε_r ($\leq$ 2 at 25 °C)[3] of *n*-octadecane, which is the functional group of the octadecylsilyl column, indicating that our HPLC experiments are conducted in reversed-phase mode.

Table S2. Number of repetitions of site combinations for each isomer of $Au_{24}Pd(SC_2H_4Ph)_{18-n}(SC_{12}H_{25})_n$ (n = 1,2).

	i [a]		j [b]											
i or j	1	2	1	2	3	4	5	6	7	8	9	10	11	12
point group	C_s	C_{2v}	C_1	C_1	C_{2v}	C_{2h}	C_{2v}	C_1	C_s	C_s	C_s	C_s	C_s	D_{2h}
order	2	4	1	1	4	4	4	1	2	2	2	2	2	8
number of repetition of site combination [c]	12	6	24 [d]	24 [d]	6	6	6	24 [d]	12	12	12	12	12	3

[a]Index of isomer in Figure 7(a). [b]Index of isomer in Figure 7(b). [c]Vertical axis in Figure 7(c)(d). [d]These values include racemates caused by the position of two ligands, which could not be separated in our experiments.

Table S3. Assignments of peaks in chromatogram of $Au_{24}Pd(SC_2H_4Ph)_{16}(SC_{12}H_{25})_2$.

retention time (min) [a]	k [b]	j [c]	exchanged sites [d]
66.76	1	3, 4, or 5	2 core
67.43	2	1 or 2	2 core
67.69	3	6	1 core + 1 apex
67.71	4	12	2 apex
67.89	5	3, 4, or 5	2 core
68.11	6	3, 4, or 5	2 core
68.69	7	1 or 2	2 core
68.73	8	7, 8, 9, or 10	1 core + 1 apex
68.76	9	7, 8, 9, or 10	1 core + 1 apex
69.25	10	11	2 apex
69.52	11	7, 8, 9, or 10	1 core + 1 apex
69.76	12	7, 8, 9, or 10	1 core + 1 apex

[a]Retention times in Figures 4(c), 6(b), 10, S11, S12, and S21. [b]Isomer index shown in Figures S11, S12, and S21. [c]Isomer index shown in Figure 7(b)(d). [d]Exchanged sites of two $SC_{12}H_{25}$.

III. Additional Figures

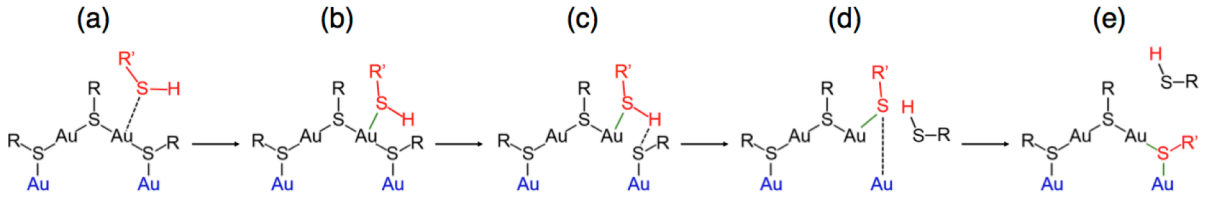

Scheme S1. Proposed mechanism in ligand exchange reaction between $Au_{24}Pd(SC_2H_4Ph)_{18}$ and $C_{12}H_{25}SH$. R and R' represent C_2H_4Ph and $C_{12}H_{25}$, respectively.

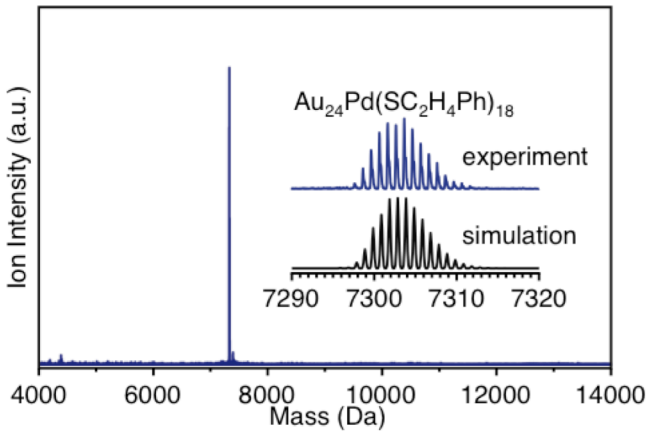

Figure S1. Negative-ion MALDI mass spectrum of $Au_{24}Pd(SC_2H_4Ph)_{18}$. Inset compares experimental and simulated results obtained using "Isotope Pattern Simulator 1.4.2.6103 (JEOL)".

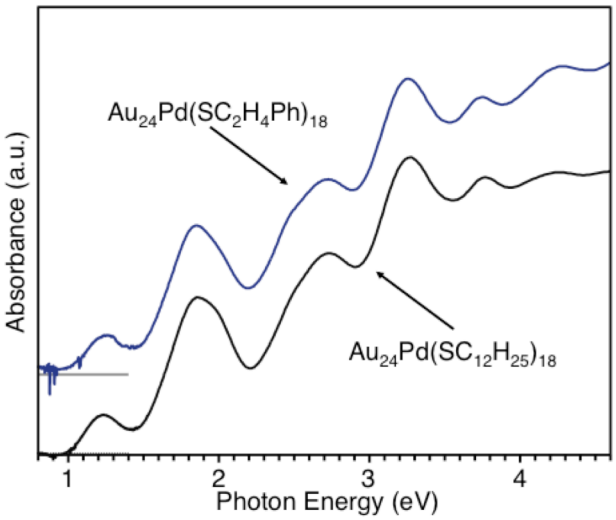

Figure S2. Optical absorption spectra of dichloromethane solutions of $Au_{24}Pd(SC_2H_4Ph)_{18}$ and $Au_{24}Pd(SC_{12}H_{25})_{18}$. Previous studies revealed that $Au_{24}Pd(SC_{12}H_{25})_{18}$ has a geometrical structure in which the central Au of $Au_{25}(SR)_{18}$ is replaced with Pd (Figure 1).[4,5] The similarity in optical absorption spectra between $Au_{24}Pd(SC_2H_4Ph)_{18}$ and $Au_{24}Pd(SC_{12}H_{25})_{18}$ indicates that $Au_{24}Pd(SC_2H_4Ph)_{18}$ also has the framework structure shown in Figure 1(a). Thus, the framework structure of $Au_{24}Pd(SC_2H_4Ph)_{18}$ protected with phenylethanethiolates is considered to be the same as that of $Au_{24}Pd(SC_{12}H_{25})_{18}$ protected with alkanethiolates. With respect to $Au_{25}(SR)_{18}$, this similarity in framework structure has been verified experimentally using single crystal X-ray crystallography of $Au_{25}(SC_2H_4Ph)_{18}$ (refs. 6,7) and $Au_{25}(SC_2H_5)_{18}$ (ref. 8).

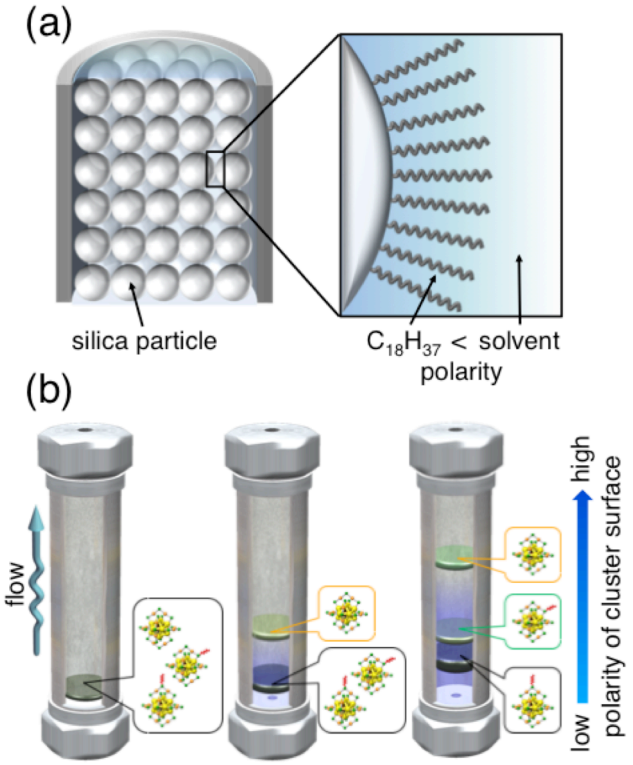

Figure S3. Schematic of (a) column and (b) elution method used for RP-HPLC.

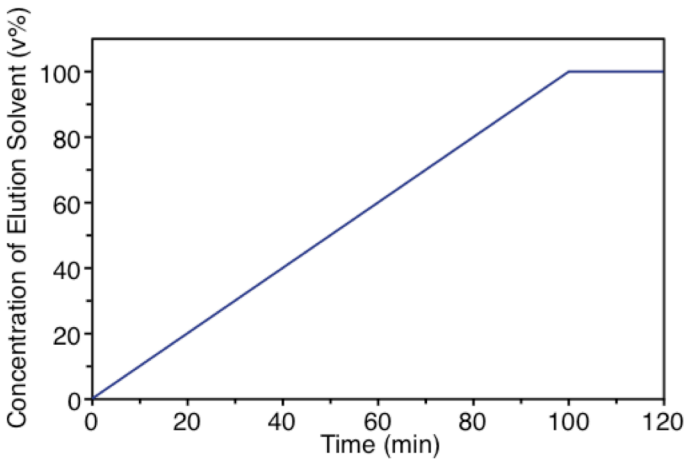

Figure S4. Gradient program used for substitution of the mobile phase. The mobile phase was generally substituted from 100% of the adsorption solvent (acetonitrile) to 100% of the elution solvent (acetone) within 100 min.

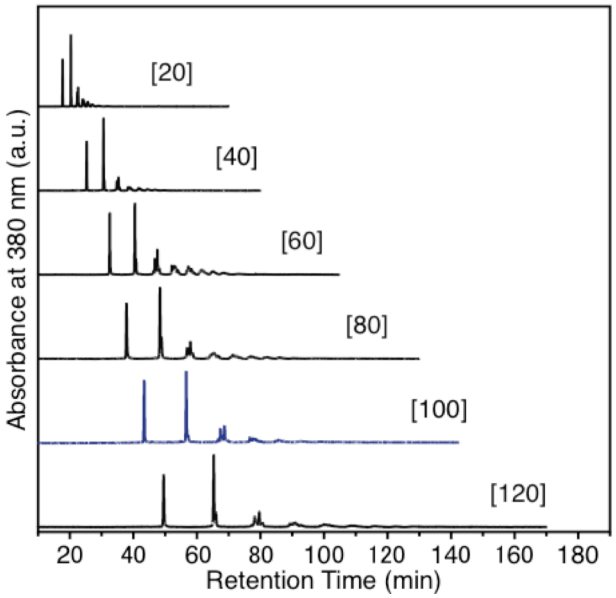

Figure S5. Chromatograms for different mobile phase substitution times. The number in parentheses ([ ]) indicates the substitution time (min). The subpeaks result from the high-resolution separation of main peaks attributed to each $Au_{24}Pd(SC_2H_4Ph)_{18-n}(SC_{12}H_{25})_n$.

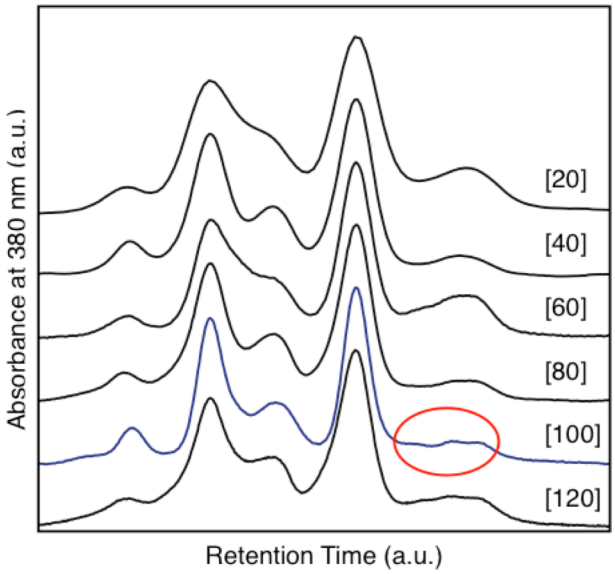

Figure S6. Chromatograms of the region of $Au_{24}Pd(SC_2H_4Ph)_{16}(SC_{12}H_{25})_2$ dependent on substitution time of the mobile phase. The horizontal axis is in arbitrary units to compare the feature of each chromatogram. The peak separation was improved with substitution time from [20]–[100] (see peaks circled in red line). However, further improvement was not observed clearly for a substitution time longer than 100 min. Thus, in this study, most chromatograms were measured using a substitution time of 100 min.

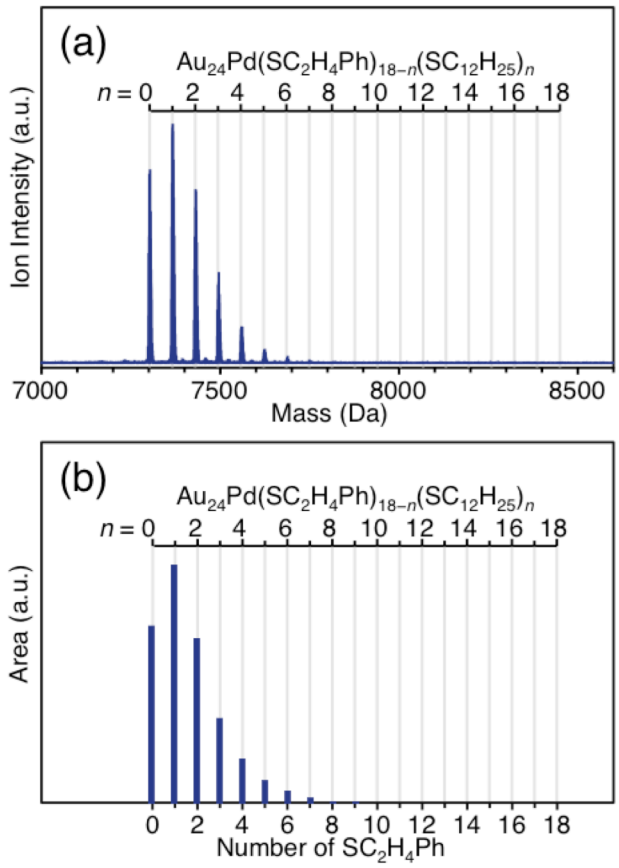

Figure S7. Comparison between (a) negative-ion MALDI mass spectrum and (b) sum of peak area of $Au_{24}Pd(SC_2H_4Ph)_{18-n}(SC_{12}H_{25})_n$ (n = 0–7) observed in the chromatogram. Peak distributions in the mass spectrum were well reproduced by the chromatogram.

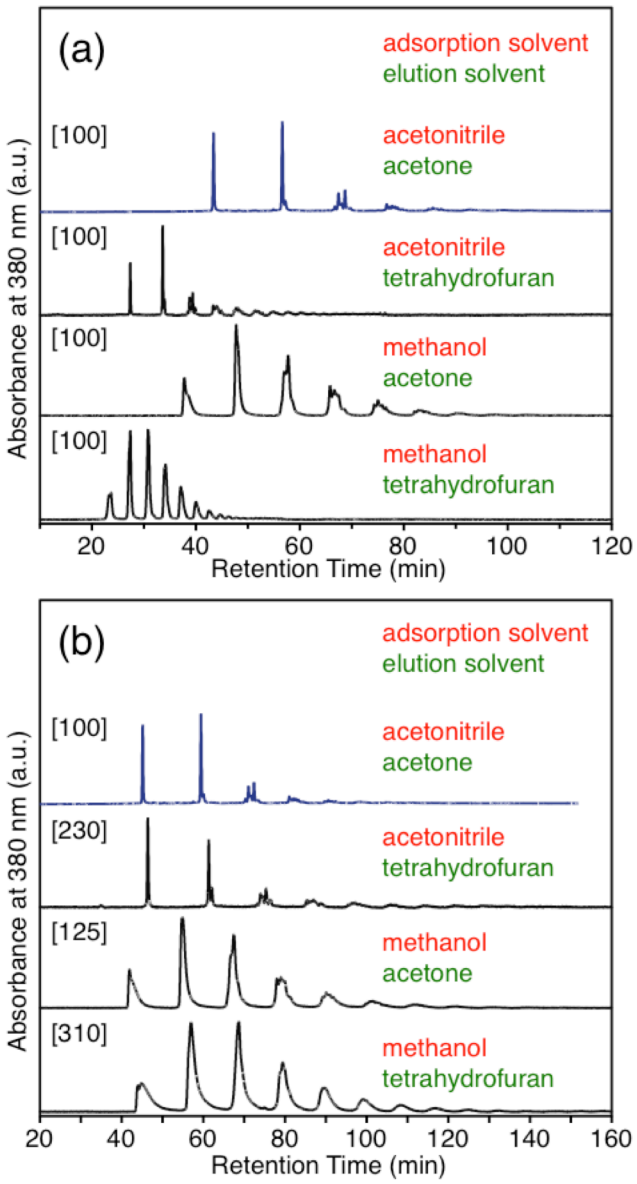

Figure S8. Chromatograms of $Au_{24}Pd(SC_2H_4Ph)_{18-n}(SC_{12}H_{25})_n$ (n = 0–7) observed for different combinations of adsorption and elution solvents. The number in parentheses ([ ]) indicates the substitution time (min) of the mobile phase from 100% adsorption solvent to 100% elution solvent. In (a), all chromatograms have the same substitution time of 100 min. In (b), different substitution times were used to elute samples with a similar retention time. The (b) indicates that the improvement achieved by using acetonitrile and acetone as adsorption and elution solvent, respectively, is not merely because of the extension of retention time caused by a difference in $Au_{24}Pd(SC_2H_4Ph)_{18-n}(SC_{12}H_{25})_n$ solubility into the mobile phase.

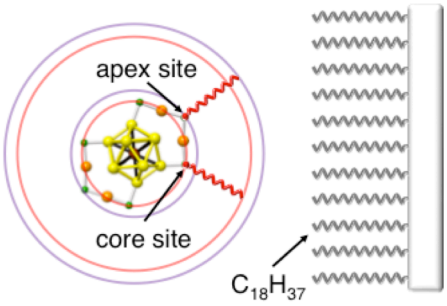

Figure S9. Schematic of ligand position in $Au_{24}Pd(SC_2H_4Ph)_{17}(SC_{12}H_{25})$. This structure is unoptimized and is shown for illustration purposes.

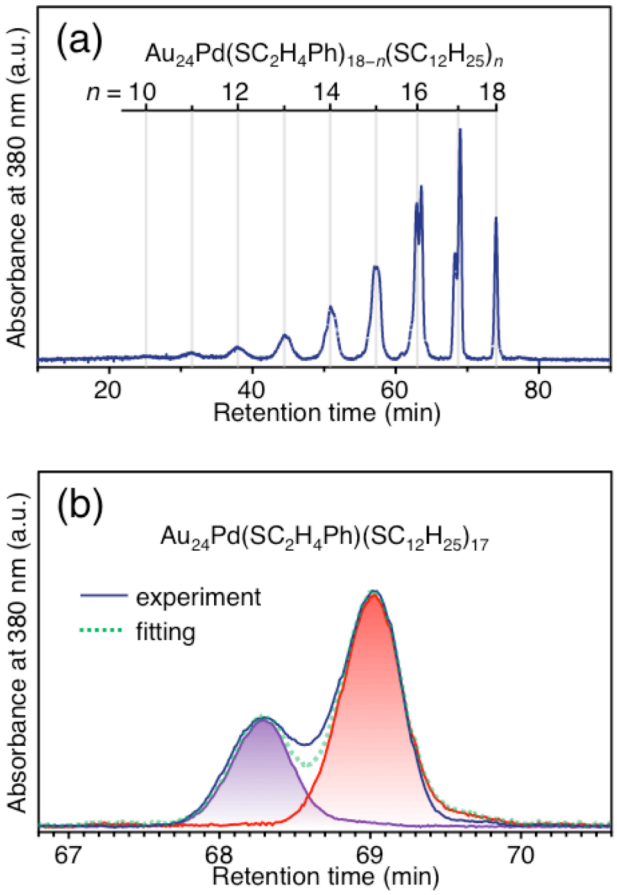

Figure S10. Chromatogram of $Au_{24}Pd(SC_2H_4Ph)_{18-n}(SC_{12}H_{25})_n$ (n = 11–18) left in toluene for 9 h; (a) wide region and (b) enlarged view of $Au_{24}Pd(SC_2H_4Ph)(SC_{12}H_{25})_{17}$ with the curve-fitting result. This chromatogram was obtained with acetone and a mixture of acetonitrile and toluene as adsorption and elution solvent, respectively, to dissolve $Au_{24}Pd(SC_2H_4Ph)_{18-n}(SC_{12}H_{25})_n$ (n = 11–18) in which many $SC_{12}H_{25}$ moieties were exchanged. In (b), $Au_{24}Pd(SC_2H_4Ph)(SC_{12}H_{25})_{17}$ was separated into two peaks with area ratios of 5.6:12.0, namely, nearly 1:2. By considering the isomer ratio, the peaks at 68.31 min and 69.03 min could be attributed to isomers in which SC_2H_4Ph exists at the apex and core sites, respectively. Thus, $Au_{24}Pd(SC_2H_4Ph)(SC_{12}H_{25})_{17}$ that includes the remaining SC_2H_4Ph at the apex site elutes earlier than that including the remaining SC_2H_4Ph at the core site. In the former (apex-site isomer), the SC_2H_4Ph, which has a weaker interaction with the stationary phase than $SC_{12}H_{25}$, is expected to exist more exteriorly (Figure 1(a)) than in the latter (core-site isomer). In this case, the apex-site isomer interacts less efficiently with the stationary phase because of this difference and therefore elutes earlier than the core-site isomer. This result is consistent with that on $Au_{24}Pd(SC_2H_4Ph)_{17}(SC_{12}H_{25})$ (Figure 4(b)), supporting our assignments of chromatogram and interpretation of elution order.

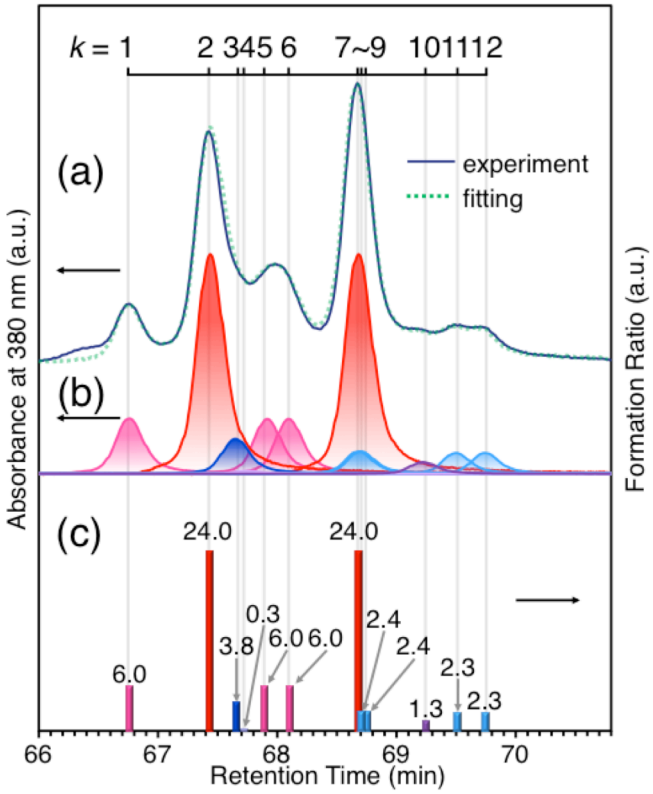

Figure S11. Curve fitting results for chromatogram of the region of $Au_{24}Pd(SC_2H_4Ph)_{16}(SC_{12}H_{25})_2$ (Figure 4(c)) of $Au_{24}Pd(SC_2H_4Ph)_{18-n}(SC_{12}H_{25})_n$ obtained just after the reaction; (a) comparison between experimental chromatogram and fitting results, (b) peak area of each isomer obtained by fitting, and (c) formation ratio of each isomer obtained by fitting. In this fitting, the peak structure used for fitting is based on the peak structure of $Au_{24}Pd(SC_2H_4Ph)_{18}$ of Figure 4(a), because the peak structure in the chromatogram is not a symmetrical curve (see Figure 4(a)). The main peaks could be curve-fitted by isomers with an intensity ratio of 24:24:6:6:6. The assignment of other peaks is described in the caption of Figure S12 and Table S3. On the basis of our tentative assignments (Figure S12 and Table S3), the isomers including two $SC_{12}H_{25}$ at the core sites (isomer index j = 1–5; red or pink bars) are estimated to be included with the ratio of 81.7% in this sample, by dividing the summation of the intensities of red and pinks bars (66.0 = 6.0 + 24.0 + 6.0 + 6.0 + 24.0) with the summation of the intensities of all peaks (80.8 = 6.0 + 24.0 + 3.8 + 0.3 + 6.0 + 6.0 + 24.0 + 2.4 + 2.4 + 1.3 + 2.3 + 2.3). The initial exchange occurs at a core site with the possibility of 93.0% as shown in Figure 4(b). Thus, the possibility that the second $SC_{12}H_{25}$ is exchanged with the remaining 11 SC_2H_4Ph of the core sites of $Au_{24}Pd(SC_2H_4Ph)_{17}(SC_{12}H_{25})$ of the core-site isomer is calculated to be 87.7%, by dividing 81.7 by 93.0. This indicates that the second exchange still occurs preferentially at the core site, although the priority is slightly less at the second exchange (87.7%) than the initial exchange (93.0%).

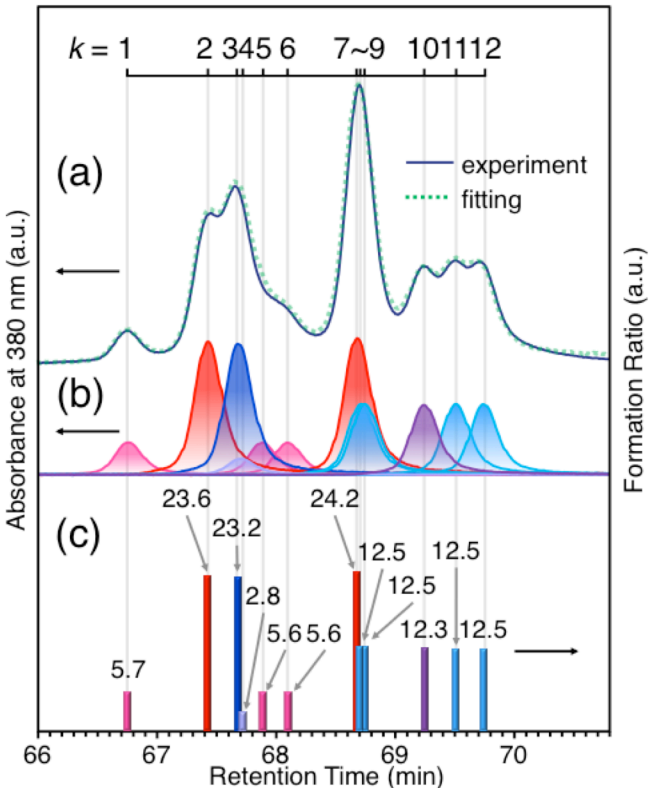

Figure S12. Curve fitting results for chromatogram of the region of $Au_{24}Pd(SC_2H_4Ph)_{16}(SC_{12}H_{25})_2$ of the $Au_{24}Pd(SC_2H_4Ph)_{18-n}(SC_{12}H_{25})_n$ standing in acetone for 9 h (Figure 6(b)); (a) comparison between experimental chromatogram and fitting results, (b) the peak area of each isomer obtained by fitting, and (c) formation ratio of each isomer obtained by fitting. In this fitting, the peak structure used for fitting is based on the peak structure of $Au_{24}Pd(SC_2H_4Ph)_{18}$ shown in Figure 4(a), because the peak structure in the chromatogram does not show a symmetrical curve (see Figure 4(a)). The observed chromatogram (Figure 6(b)) could be fitted with 12 peaks having an area ratio of nearly 24:24:6:6:6:24:12:12:12:12:12:3, which is the ratio of the number of the repetition of the site combination of 12 coordination isomers listed in Figure 7(b)(d). In these figures, the isomer index k is not consistent with the isomer index j shown in Figure 7(b)(d), because it is difficult currently to relate these peaks perfectly with the isomers listed in Figure 7(b)(d). However, a comparison with Figure 4(c) implies that the two red peaks (k = 2,7) are attributed to the isomers of isomer index j = 1,2 and the three pink peaks (k = 1,5,6) are attributed to the isomers of isomer index j = 3–5. The light purple peak (k = 4) could be attributed to the isomers of isomer index j = 12 on the basis of the formation ratio of this isomer. The purple peak (k = 10) is presumed to be attributed to the isomers of isomer index j = 11 in which two $SC_{12}H_{25}$ are exchanged at the apex sites because this peak was weak immediately after the ligand-exchange reaction, as shown in Figure S11. On the basis of these assignments, the blue peak (k = 3) could be assigned to isomers of the isomer index j = 6, and the four light blue peaks (k = 8,9,11,12) could be assigned to isomers of the isomer index j = 7–10. The last five isomers (k = 3,8,9,11,12) were observed as a main species in $Au_{24}Pd(SC_2H_4Ph)_{16}(SC_{12}H_{25})_2$ generated by isomer-separated apex-type $Au_{24}Pd(SC_2H_4Ph)_{17}(SC_{12}H_{25})$ (Figures 9 and S21). In this product, the main $Au_{24}Pd(SC_2H_4Ph)_{16}(SC_{12}H_{25})_2$ is expected to be the isomer that contains one $SC_{12}H_{25}$ at the core site and one $SC_{12}H_{25}$ at the apex site (j = 6–10). Thus, the above assignments are also supported by Figures 9 and S21. The assignment of each peak discussed in this caption is summarized in Table S3. On the whole, the retention times of $Au_{24}Pd(SC_2H_4Ph)_{16}(SC_{12}H_{25})_2$, in which two $SC_{12}H_{25}$ are exchanged at core sites, were shorter than those of $Au_{24}Pd(SC_2H_4Ph)_{16}(SC_{12}H_{25})_2$, in which the exchange occurs at the apex site(s) (Table S3). These results are consistent with the results on $Au_{24}Pd(SC_2H_4Ph)_{17}(SC_{12}H_{25})$ (Figure 4(b)).

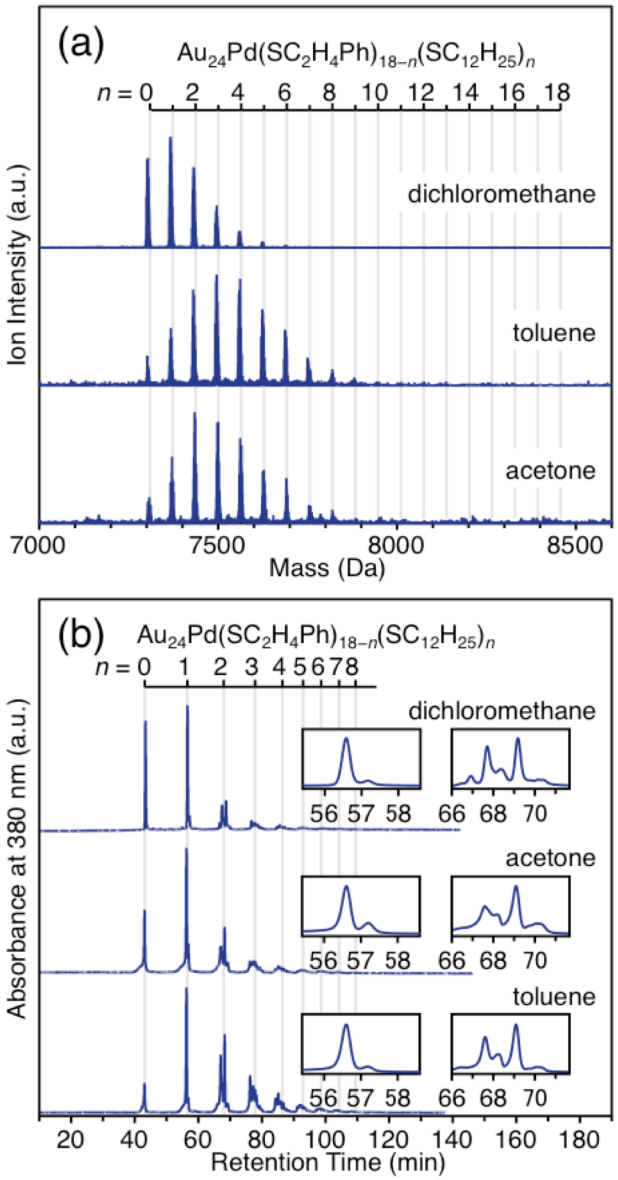

Figure S13. (a) Negative-ion MALDI mass spectra and (b) chromatograms of samples of $Au_{24}Pd(SC_2H_4Ph)_{18-n}(SC_{12}H_{25})_n$ obtained by reaction between $Au_{24}Pd(SC_2H_4Ph)_{18}$ and $C_{12}H_{25}SH$ in different solvents (dichloromethane, toluene, or acetone).

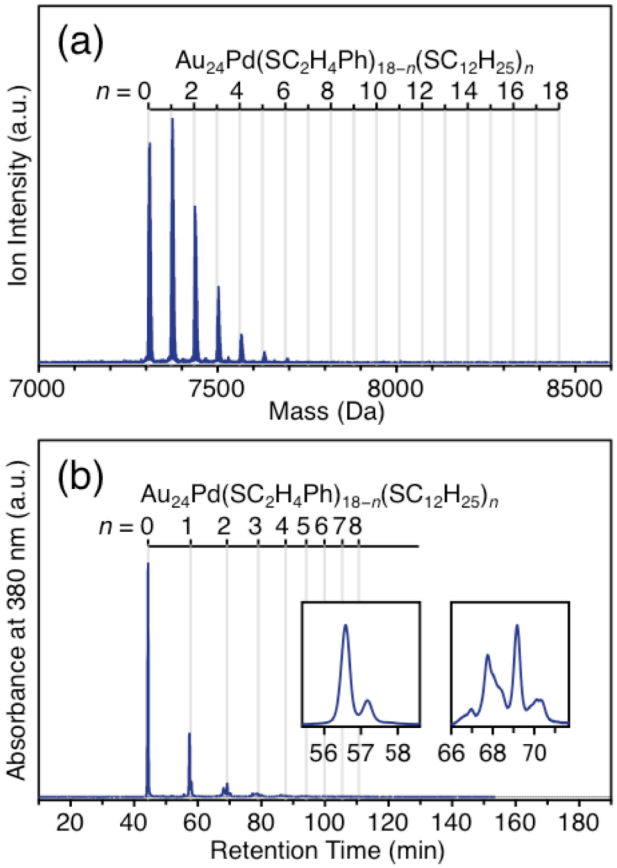

Figure S14. (a) Negative-ion MALDI mass spectrum and (b) chromatogram of sample of $Au_{24}Pd(SC_2H_4Ph)_{18-n}(SC_{12}H_{25})_n$ obtained by reaction between $Au_{24}Pd(SC_2H_4Ph)_{18}$ and $C_{12}H_{25}SH$ without a solvent.

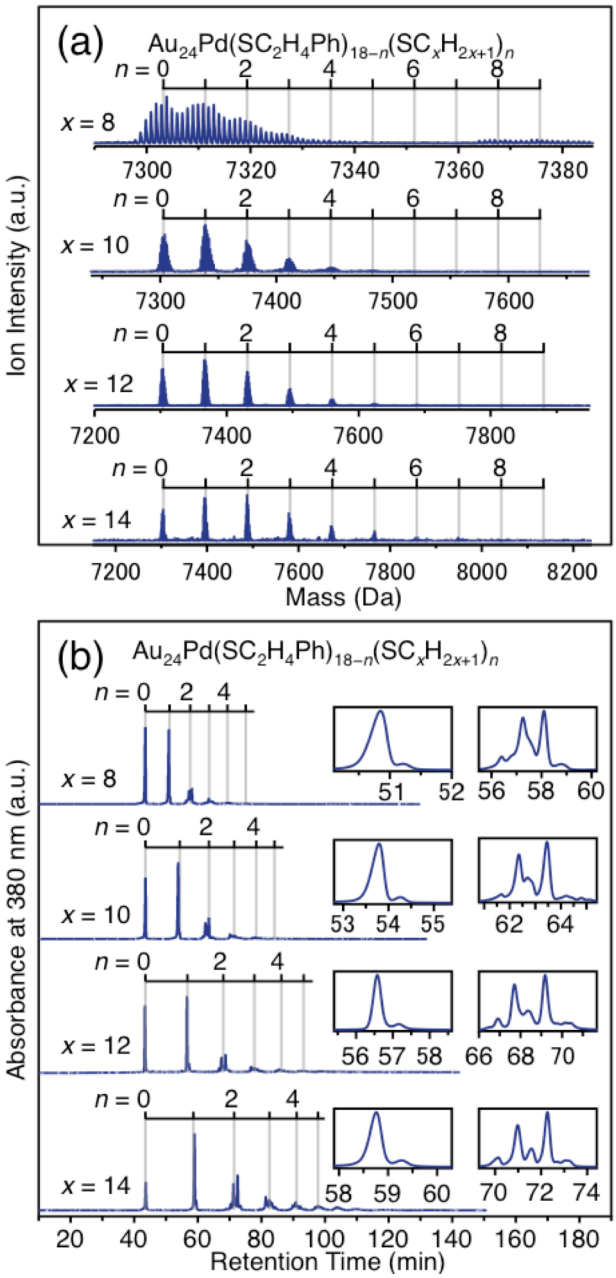

Figure S15. (a) Negative-ion MALDI mass spectra and (b) chromatograms of samples of $Au_{24}Pd(SC_2H_4Ph)_{18-n}(SC_xH_{2x+1})_n$ (x = 8, 10, 12, or 14) obtained by reaction between $Au_{24}Pd(SC_2H_4Ph)_{18}$ and $C_xH_{2x+1}SH$ in dichloromethane.

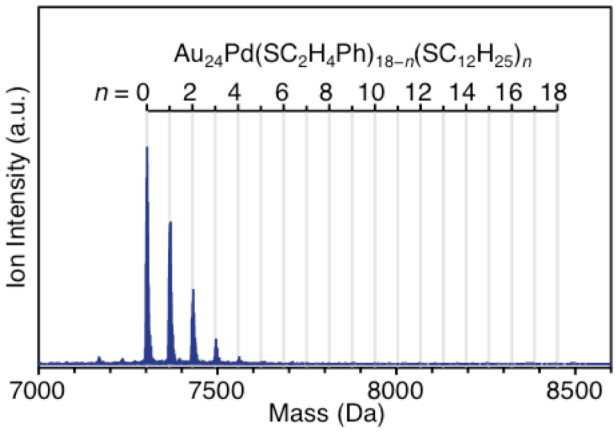

Figure S16. Negative-ion MALDI mass spectrum of sample of $Au_{24}Pd(SC_2H_4Ph)_{18-n}(SC_{12}H_{25})_n$ obtained by reaction between $Au_{24}Pd(SC_2H_4Ph)_{18}$ and $(C_{12}H_{25}S)_2$ in dichloromethane.

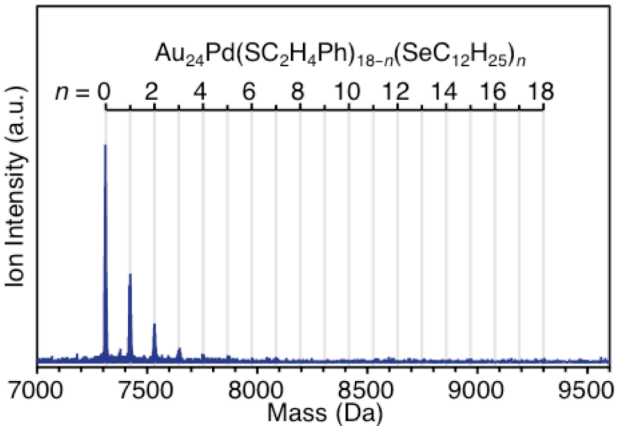

Figure S17. Negative-ion MALDI mass spectrum of sample of $Au_{24}Pd(SC_2H_4Ph)_{18-n}(SeC_{12}H_{25})_n$ obtained by reaction between $Au_{24}Pd(SC_2H_4Ph)_{18}$ and $(C_{12}H_{25}Se)_2$ in dichloromethane.

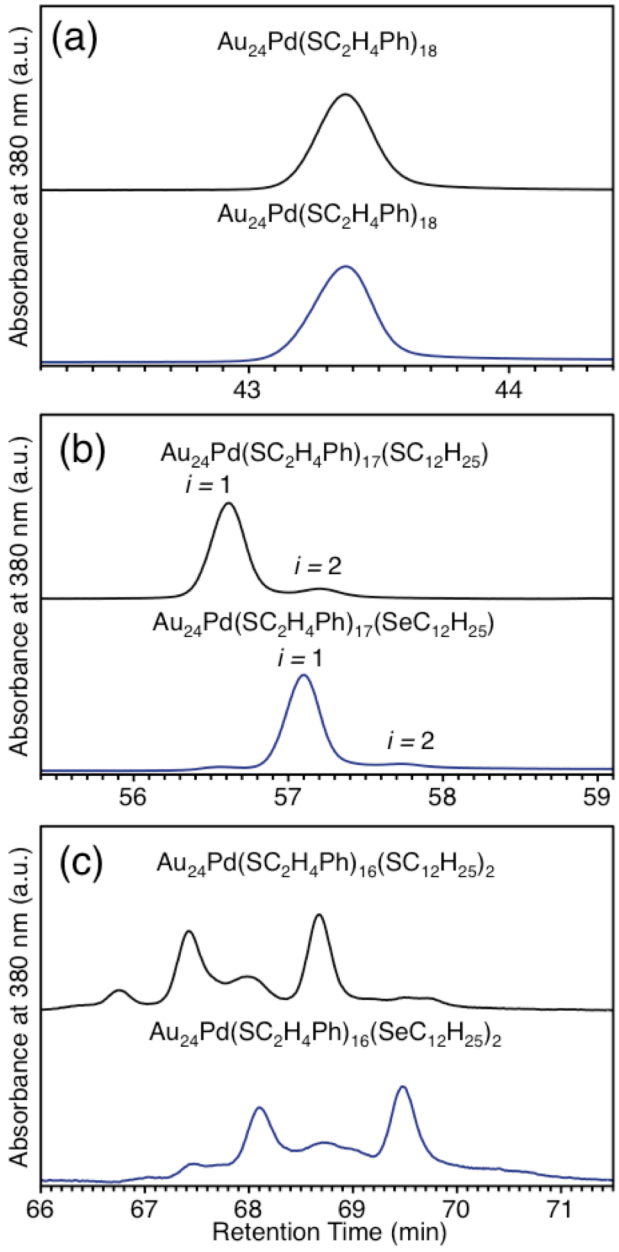

Figure S18. Comparison of chromatograms between $Au_{24}Pd(SC_2H_4Ph)_{18-n}(SC_{12}H_{25})_n$ and $Au_{24}Pd(SC_2H_4Ph)_{18-n}(SeC_{12}H_{25})_n$; (a) n = 0, (b) n = 1, and (c) n = 2. $Au_{24}Pd(SC_2H_4Ph)_{18-n}(SeC_{12}H_{25})_n$ (n = 1,2) eluted with a longer retention time than $Au_{24}Pd(SC_2H_4Ph)_{18-n}(SC_{12}H_{25})_n$ (n = 1,2). This difference was not observed in a previous study[9] in which the clusters were eluted within a shorter retention time using a different gradient program. In $Au_{24}Pd(SC_2H_4Ph)_{18-n}(SeC_{12}H_{25})_n$ (n = 1,2), $C_{12}H_{25}$ is expected to exist more exteriorly than in $Au_{24}Pd(SC_2H_4Ph)_{18-n}(SC_{12}H_{25})_n$ (n = 1,2), because of the difference in atomic radius between Se (1.17 Å) and S (1.04 Å). Thus, $Au_{24}Pd(SC_2H_4Ph)_{18-n}(SeC_{12}H_{25})_n$ (n = 1,2) is expected to interact more efficiently with the stationary phase because the $C_{12}H_{25}$ exists more exteriorly. This is expected to lead to a slightly longer retention time than $Au_{24}Pd(SC_2H_4Ph)_{18-n}(SC_{12}H_{25})_n$ (n = 1,2).

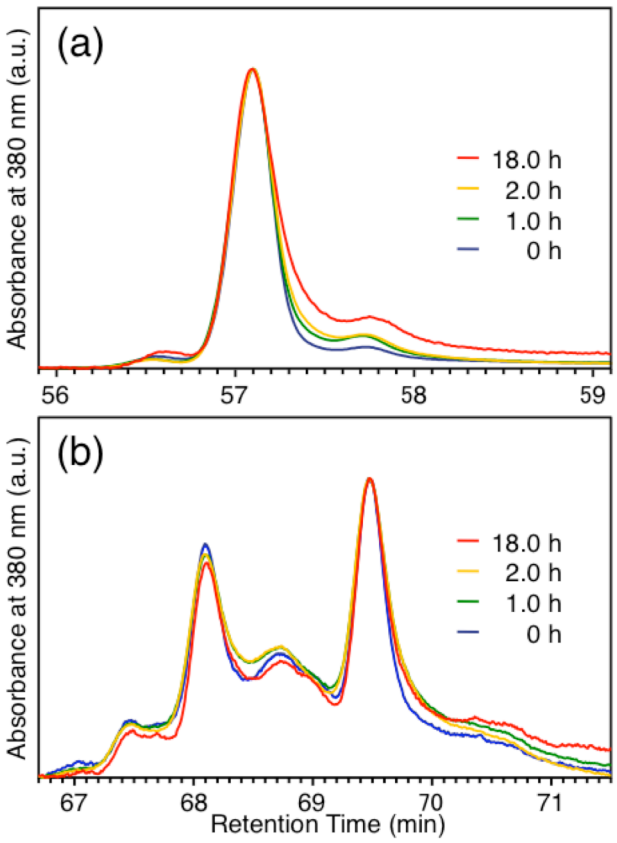

Figure S19. Time dependence of chromatograms of $Au_{24}Pd(SC_2H_4Ph)_{18-n}(SeC_{12}H_{25})_n$ standing in acetone for the region of (a) $Au_{24}Pd(SC_2H_4Ph)_{17}(SeC_{12}H_{25})$ and (b) $Au_{24}Pd(SC_2H_4Ph)_{16}(SeC_{12}H_{25})_2$. In these cases, only slight changes were observed in contrast with the case of $Au_{24}Pd(SC_2H_4Ph)_{18-n}(SC_{12}H_{25})_n$ (Figure 6) probably because of the stronger Au-selenolate bonds.[10]

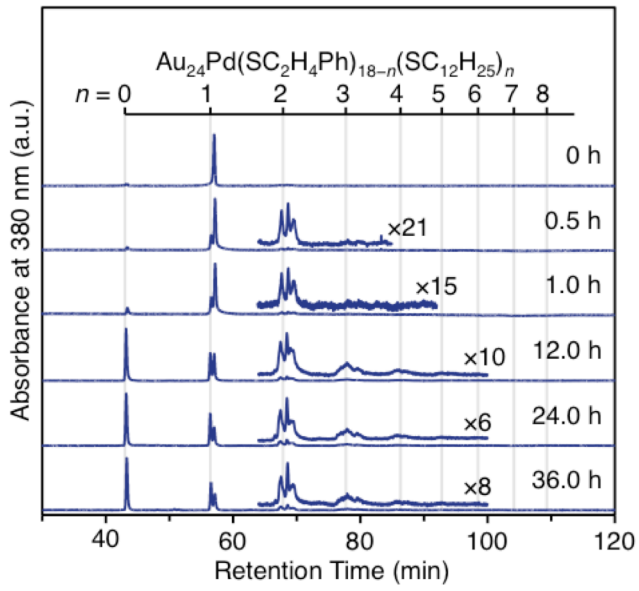

Figure S20. Time dependences of chromatograms of isomer-separated apex-site type $Au_{24}Pd(SC_2H_4Ph)_{17}(SC_{12}H_{25})$ standing in acetone.

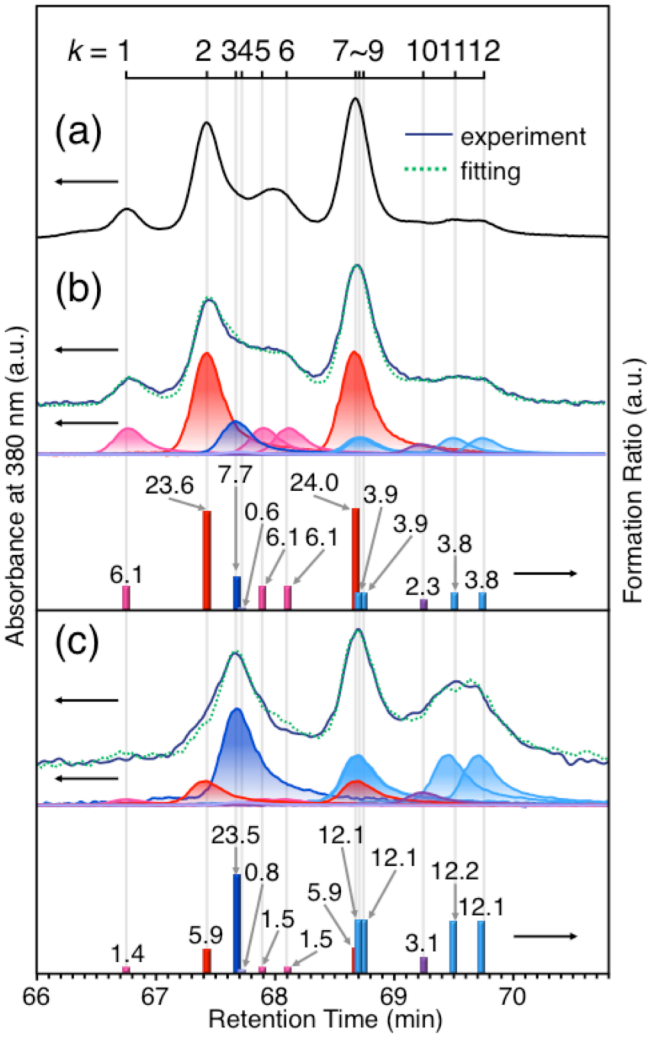

Figure S21. Chromatograms of $Au_{24}Pd(SC_2H_4Ph)_{16}(SC_{12}H_{25})_2$; $Au_{24}Pd(SC_2H_4Ph)_{16}(SC_{12}H_{25})_2$ obtained by (a) the reaction between $Au_{24}Pd(SC_2H_4Ph)_{18}$ and $C_{12}H_{25}SH$ in dichloromethane (Figure 4(c)), (b) the standing of core-site type $Au_{24}Pd(SC_2H_4Ph)_{17}(SC_{12}H_{25})$ in acetone for 0.5 h (Figure 9), and (c) the standing of apex-site type $Au_{24}Pd(SC_2H_4Ph)_{17}(SC_{12}H_{25})$ in acetone for 0.5 h (Figure S20). For (b)(c), curve fitting results of the chromatograms and the formation ratio of each isomer of isomer index k = 1–12 (Table S3) are also shown. On the basis of the assignments of Figure S12 (Table S3), it is estimated that the sample of (b) contains 71.6% of isomers with two $SC_{12}H_{25}$ at the core sites (isomer index j = 1–5; red or pink bars), 25.2% of that having one $SC_{12}H_{25}$ at the core site and one $SC_{12}H_{25}$ at the apex site (isomer index j = 6–10; blue or light blue bars), and 3.2% of that having two $SC_{12}H_{25}$ at the apex site (j = 11,12), whereas the sample of (c) contains 17.5% of the isomers having two $SC_{12}H_{25}$ at the core sites (isomer index j = 1–5; red or pink bars), 78.3% of that having one $SC_{12}H_{25}$ at the core site and one $SC_{12}H_{25}$ at the apex site (isomer index j = 6–10; blue or light blue bars), and 4.2% of that having two $SC_{12}H_{25}$ at the apex site (j = 11,12).

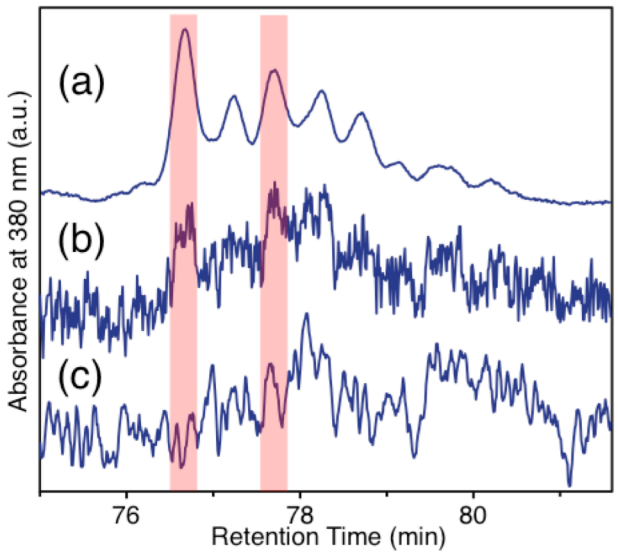

Figure S22. Chromatograms of the region of $Au_{24}Pd(SC_2H_4Ph)_{15}(SC_{12}H_{25})_3$ obtained by (a) reaction between $Au_{24}Pd(SC_2H_4Ph)_{18}$ and $C_{12}H_{25}SH$ in dichloromethane (Figure 4(c)), (b) the standing of core-site type $Au_{24}Pd(SC_2H_4Ph)_{17}(SC_{12}H_{25})$ in acetone for 0.5 h (Figure 9), and (c) the standing of apex-site type $Au_{24}Pd(SC_2H_4Ph)_{17}(SC_{12}H_{25})$ in acetone for 0.5 h (Figure S20). The main peaks observed in (a) marked with the red bars also appear in (b), whereas they are weak in (c).

IV. References

1. Armstrong, M. A. *Groups and Symmetry*; Springer-Verlag: New York, 1988.
2. Lide, D. R. *CRC Handbook of Chemistry and Physics,* 89th ed.; CRC Press; New York, 2008; 6-p 154, 6-p 197.
3. Eisenthal, K. B.; Hochstrasser, R. M.; Kaiser, W.; Laubereau, A. *Picosecond Phenomena III: Proceedings of the Third International Conference on Picosecond Phenomena Garmisch-Partenkirchen, Fed. Rep. of Germany June 16-18, 1982*; Springer-Verlag; New York; 1982; p 276.
4. Negishi, Y.; Kurashige, W.; Niihori, Y.; Iwasa, T.; Nobusada, K. Isolation, Structure, and Stability of a Dodecanethiolate-Protected Pd_1Au_{24} Cluster. *Phys. Chem. Chem. Phys.* **2010**, *12*, 6219–6225.
5. Negishi, Y.; Kurashige, K.; Kobayashi, Y.; Yamazoe, Y.; Kojima, N.; Seto, M; Tsukuda, T. Formation of a $Pd@Au_{12}$ Superatomic Core in $Au_{24}Pd_1(SC_{12}H_{25})_{18}$ Probed by ^{197}Au Mössbauer and Pd K-Edge EXAFS Spectroscopy. *J. Phys. Chem. Lett.* **2013**, *4*, 3579–3583.
6. Heaven, M. W.; Dass, A.; White, P. S.; Holt, K. M.; Murray, R. W. Crystal Structure of the Gold Nanoparticle $[N(C_8H_{17})_4][Au_{25}(SCH_2CH_2Ph)_{18}]$. *J. Am. Chem. Soc.* **2008**, *130*, 3754–3755.
7. Zhu, M.; Aikens, C. M.; Hollander, F. J.; Schatz, G. C.; Jin, R. Correlating the Crystal Structure of A Thiol-Protected Au_{25} Cluster and Optical Properties. *J. Am. Chem. Soc.* **2008**, *130*, 5883–5885.
8. Dainese, T.; Antonello, S.; Gascón, J. A.; Pan, F.; Perera, N. V.; Ruzzi, M.; Venzo, A.; Zoleo, A.; Rissanen, K.; Maran, F. $Au_{25}(SEt)_{18}$, a Nearly Naked Thiolate-Protected Au_{25} Cluster: Structural Analysis by Single Crystal X-ray Crystallography and Electron Nuclear Double Resonance. *ACS Nano* **2014**, *8*, 3904–3912.
9. Niihori, Y.; Matsuzaki, M.; Uchida, C.; Negishi, Y. Advanced Use of High-Performance Liquid Chromatography for Synthesis of Controlled Metal Clusters. *Nanoscale* **2014**, *6*, 7889–7896.
10. Kurashige, W.; Yamaguchi, M.; Nobusada, K.; Negishi, Y. Ligand-Induced Stability of Gold Nanoclusters: Thiolate versus Selenolate. *J. Phys. Chem. Lett.* **2012**, *3*, 2649–2652.